Tellus (1984), *36A*, 446–457

Stratocumulus cloud deepening through entrainment

By DAVID A. RANDALL, *Goddard Laboratory for Atmospheric Sciences, NASA/Goddard Space Flight Center, Greenbelt, Md 20771, USA*

(Manuscript received February 14; in final form May 8, 1984)

ABSTRACT

It is shown that under a fairly wide range of realistic conditions, stratocumulus cloud-top entrainment actually tends to deepen an existing cloud layer, or tends to produce clouds in an unsaturated mixed layer, even though the entrained air is warmer and drier than the mixed-layer air. These results do not depend on any particular theory of what determines the entrainment rate; they imply that the cloud-top entrainment instability discussed by Randall and Deardorff does not necessarily tend to destroy a layer cloud; it sometimes only makes the cloud deepen. Examples are presented, using the representative soundings of McClatchey et al., the marine-layer data of Neiburger et al., and results from a simulation produced with the UCLA general circulation model.

1. Introduction

The air above stratocumulus cloud top is typically observed to have a much higher potential temperature and a much lower mixing ratio than the air within the cloud (Brost et al., 1982; Mahrt and Paumier, 1982). Therefore it has often been assumed that cloud-top entrainment tends to destroy the cloud layer (Lilly, 1968). However, this assumption is not always justified. Cloud-top entrainment tends to raise the cloud-base level by diluting the cloud with warm dry air, but it also tends to lift cloud-top height. In this paper, I demonstrate that under many realistic conditions the latter effect actually dominates, i.e., the net effect of entrainment is that the cloud top tends to rise more quickly than the cloud base, so that the cloud depth tends to increase with time. This process can be called "cloud deepening through entrainment" (CDE).

2. The effects of entrainment on the liquid water mixing ratio at stratocumulus top

For a stratocumulus cloud in the upper portion of a well-mixed layer (Lilly, 1968), the cloud-top liquid water mixing ratio, l_B, increases monotonically with cloud depth. As discussed in the Appendix, l_B depends only on the moist static energy, h_M, the total water mixing ratio, r_M, the mixed layer's pressure depth, δp_M, and the surface pressure, p_S. By the chain rule, we can write

$$\frac{\partial l_B}{\partial t} = \left(\frac{\partial l_B}{\partial h_M}\right)_{r_M,\,\delta p_M} \frac{\partial h_M}{\partial t} + \left(\frac{\partial l_B}{\partial r_M}\right)_{h_M,\,\delta p_M} \frac{\partial r_M}{\partial t} + \left(\frac{\partial l_B}{\partial \delta_{pM}}\right)_{h_M,\,r_M} \frac{\partial \delta p_M}{\partial t} + \left(\frac{\partial l_B}{\partial p_s}\right)_{h_M,\,r_M} \frac{\partial p_S}{\partial t}. \quad (2.1)$$

For simplicity, we consider only the time rates of change associated with entrainment, i.e.

$$\frac{\partial h_M}{\partial t} = g\frac{E\Delta h}{\delta p_M}, \quad (2.2a)$$

$$\frac{\partial r_M}{\partial t} = g\frac{E\Delta r}{\delta p_M}, \quad (2.2b)$$

$$\frac{\partial \delta p_M}{\partial t} = gE, \quad (2.2c)$$

$$\frac{\partial p_S}{\partial t} = 0. \quad (2.2d)$$

Here g is the acceleration of gravity, E is the entrainment mass flux and Δh and Δr are the "jumps" of h and r respectively, across cloud top (e.g., Randall 1980).

Although we have included only entrainment terms in (2.2(a–c)), we do not mean to suggest that other terms (e.g. those due to large-scale motion or surface fluxes) are negligible. Obviously these other terms are of great importance. For example, large-scale sinking motion can cause a cloud layer to become shallower even though entrainment tends to deepen the cloud (i.e., even though CDE is occurring); surface evaporation can cause a cloud layer to deepen even though entrainment tends to make the cloud shallower (i.e., even though CDE is not occurring). These possibilities must be allowed for in a useful cloud-topped mixed-layer model (e.g., Randall, 1984). However, the purpose of this paper is to point out that the *tendencies due to entrainment* can sometimes favor an increase in cloud depth. For this reason, only entrainment terms are included in (2.2(a–c)).

Substituting (2.2(a–d)) into (2.1), multiplying by L/c_p, where L is the latent heat of condensation and c_p is the specific heat of dry air at constant pressure, and collecting terms, we obtain

$$\frac{L}{c_p}\frac{\partial l_B}{\partial t} = \frac{gE}{\partial p_M} X, \tag{2.3}$$

where

$$X = \frac{L}{c_p}\left(\frac{\partial l_B}{\partial h_M}\Delta h + \frac{\partial l_B}{\partial r_M}\Delta r + \delta p_M \frac{\partial l_B}{\partial \delta p_M}\right). \tag{2.4}$$

Expressions for $\partial l_B/\partial h_M$, $\partial l_B/\partial r_M$ and $\partial l_B/\partial \delta p_M$ are worked out in the Appendix. They are primarily functions of T_B and δp_M; their dependence on p_S is generally negligible. The first term of (2.4) can have either sign, and the second is practically always negative. The third term represents the effects of deepening the mixed layer. Because the saturation mixing ratio decreases with height, the difference between r_M and the saturation mixing ratio increases as δp_M increases. As a result, the third term of (2.4) is positive, and it is this fact that makes it possible for CDE to occur.

Let

$$\Delta\sigma_d \equiv [\Delta h - (1-\delta\varepsilon) L\Delta r]/c_p, \tag{2.5a}$$

$$\Delta\sigma_m \equiv (\beta\Delta h - \varepsilon L\Delta r)/c_p, \tag{2.5b}$$

where the positive thermodynamic coefficients δ, ε, and β are those defined by Randall (1980). As discussed in that paper, $\Delta\sigma_d < 0$ is the criterion for dry static instability at the PBL top*; $\Delta\sigma_m < 0$ is the criterion for cloud-top entrainment instability, which is a type of moist static instability associated with the evaporative cooling of entrained air (Randall, 1980; Deardorff, 1980). Of course, these stability criteria apply only in the unsaturated and saturated cases, respectively. Nevertheless, we can use (2.5(a–b)) to formally *define* both $\Delta\sigma_d$ and $\Delta\sigma_m$ whether or not the PBL top is saturated. By using (2.5), we can rewrite (2.4) as

$$X = (\Lambda_0 + \Delta\sigma_d \Lambda_d + \Delta\sigma_m \Lambda_m), \tag{2.6}$$

where

$$\Lambda_0 \equiv (L/c_p)\,\delta p_M\, \partial l_B/\partial \delta p_M, \tag{2.7a}$$

$$\Lambda_d \equiv \left(-\varepsilon L\frac{\partial l_B}{\partial h_M} - \beta\frac{\partial l_B}{\partial r_M}\right)/|-\varepsilon + \beta(1-\delta\varepsilon)|, \tag{2.7b}$$

$$\Lambda_m \equiv \left[(1-\delta\varepsilon) L\frac{\partial l_B}{\partial h_M} + \frac{\partial l_B}{\partial r_M}\right]/|-\varepsilon + \beta(1-\delta\varepsilon)|. \tag{2.7c}$$

Inspection of (2.7) shows that Λ_0 is a temperature, while Λ_d and Λ_m are non-dimensional. Fig. 1 shows Λ_0, Λ_d and Λ_m as functions of T_B and δp_M, for p_S = 1020 mb. The figure shows that $\Lambda_0 > 0$, $\Lambda_d < 0$, and $\Lambda_m > 0$. This means that increasing dry stability inhibits CDE, while increasing moist stability promotes CDE. As δp_M increases, Λ_d and Λ_m change only slightly, but Λ_0 increases significantly.

3. A stability analysis

According to (2.3), entrainment will tend to increase or decrease l_B according to whether $X > 0$ or $X < 0$. In this Section, we investigate the variability of X in the ($\Delta\sigma_d$, $\Delta\sigma_m$) plane, and interpret the results in terms of the stability of the cloud layer.

To determine X using (2.6), it is necessary to evaluate Λ_0, Λ_d, and Λ_m. For this purpose, we must choose values of T_B, δp_M, and p_S. We have

* In fact, in the absence of cloud, $\Delta\sigma_d$ is identical to ΔT_v, where T_v is the virtual temperature.

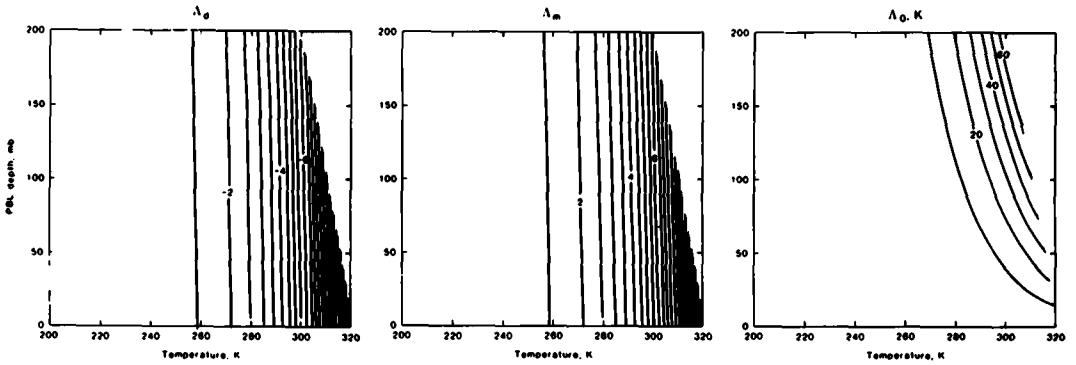

Fig. 1. Contour plots of Λ_d Λ_m, and Λ_θ, in the $(T, \delta p_M)$ plane, for p_S = 1020 mb. Contours are not plotted in the upper right-hand corner of the figure, since these combinations of T and p do not occur in the Earth's atmosphere.

Table 1. *Parameters corresponding to the results of Fig. 2 (case 1) and Fig. 3 (case 2)*

Case number	δp_M (mb)	Λ_θ (K)	Λ_d	Λ_m	γ	β	ε
1	50	5.34	−3.11	3.13	1.56	0.502	0.114
2	150	12.02	−2.46	2.51	1.07	0.575	0.110

considered the two cases summarized in Table 1. For both cases, T_S = 290 K and p_S = 1020 mb. For case 1, δp_M = 50 mb; and for Case 2, δp_M is increased to 150 mb. To evaluate T_B, we use $T_B = T_S(p_B/p_S)^\kappa$, where κ is the Poisson constant. We have evaluated X, the relative humidity above cloud-top, $\Delta h/c_p$, and Δr for cases 1 and 2. Negative values of $\Delta\sigma_d$ have not been considered, but both positive and negative values of $\Delta\sigma_m$ have been allowed. To evaluate the relative humidity above cloud top, it was necessary to choose a value of r_M. (Of course, the relative humidity above cloud top is physically independent of r_M. The apparent dependence here is an artifact of the calculation.) For this purpose, we have considered the limit of infinitesimal cloud thickness, in which $r_M = q_B^*$; this choice gives the smallest possible relative humidity above cloud top, but otherwise has no effect on the results discussed below.

The results are presented in Figs. 2, 3. No contours are plotted for the regions where the relative humidity above cloud-top is greater than 100% or less than zero; these regions are colored in black. Isopleths of X are straight lines sloping from the lower left to the upper right. Recall that CDE occurs where $X > 0$. There is a triangular region, coloured in red, within which $\Delta\sigma_m < 0$, while $X > 0$. The size of the red triangle increases as the PBL depth increases. Randall (1980) showed that cloud-top entrainment instability occurs for $\Delta\sigma_m < 0$. He suggested that under these conditions the entrainment process "runs away", since entrainment actually favors buoyant convection near cloud top. This conclusion is supported by the numerical results of Deardorff (1980), Moeng and Arakawa (1980), and Chen and Cotton (1980). Randall (1980) assumed that cloud-top entrainment instability always tends to destroy the stratocumulus layer. However, the present analysis shows that within the red triangle, the entrainment instability actually tends to deepen the cloud sheet. In this part of the domain, where CDE is active, the entrainment instability is a cloud-builder, not a cloud-destroyer.

CDE also occurs in the orange region of Figs. 2, 3, although cloud-top entrainment instability does not occur there, since $\Delta\sigma_m > 0$. CDE does not occur in the green region, but cloud-top entrainment instability does occur, so that a cloud sheet breaks up into fragments, as envisioned by Randall (1980). Neither CDE nor the entrainment instability occur in the yellow region.

Comparison of Fig. 2 with Fig. 3 shows that CDE is favored by large values of δp_M. The reason is that the drying effects of the entrained air are minimized when it is mixed through deep layer.

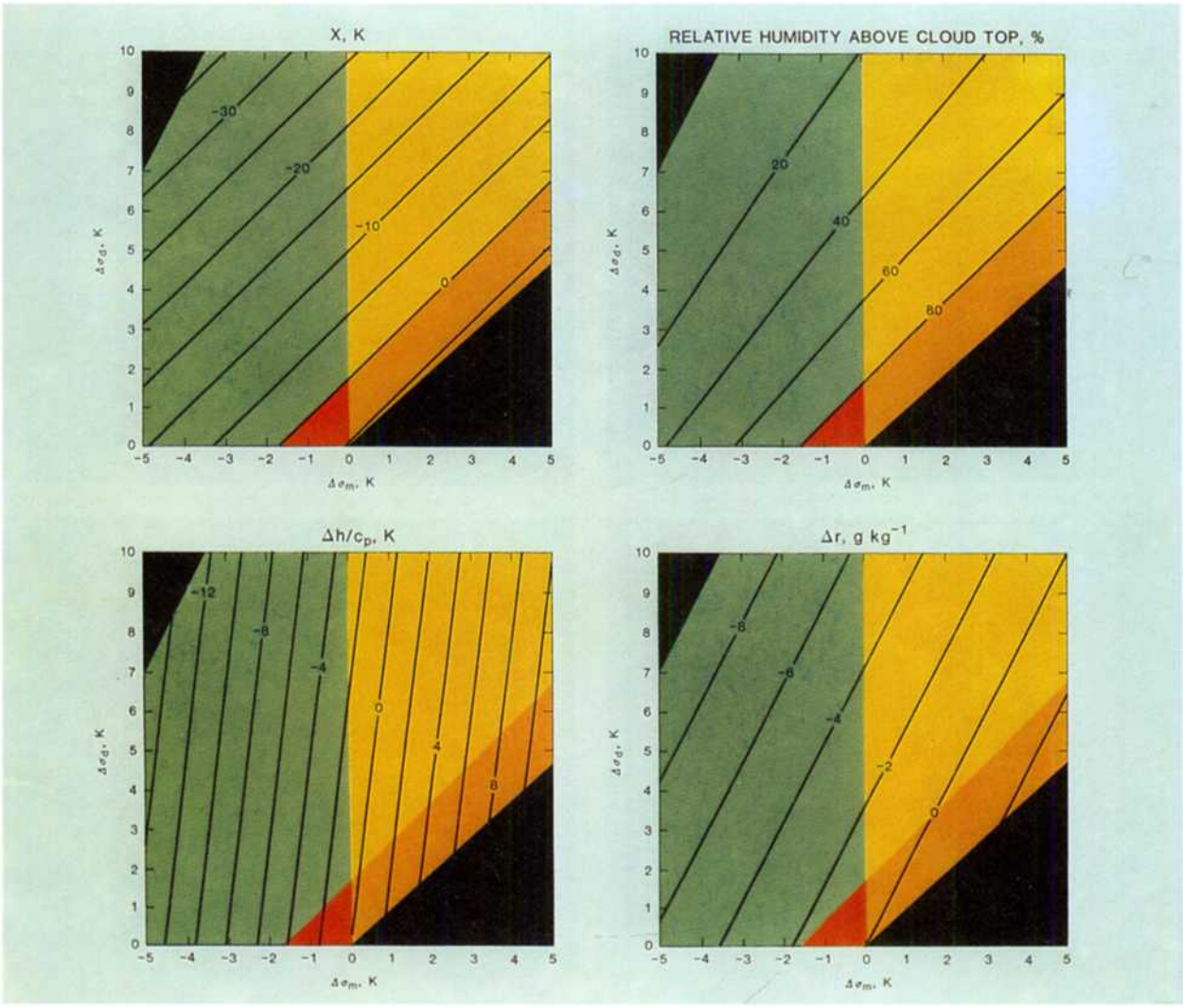

Fig. 2. Contour plot of X(K), $\Delta h/c_p$(K), Δr(g kg^{-1}), and the relative humidity above cloud-top (%), over the ($\Delta\sigma_d$, $\Delta\sigma_m$) plane, for δp_M = 50 mb and $r_M = q_B^*$. In the black regions, the relative humidity above cloud-top is either greater than 100% (lower right) or less than zero (upper left). Red denotes the region in which both CDE and cloud-top entrainment instability occur. Orange is used where CDE occurs but the entrainment instability does not. In the yellow region, neither CDE nor the entrainment instability occurs. Finally, in the green region, the entrainment instability does occur but CDE does not.

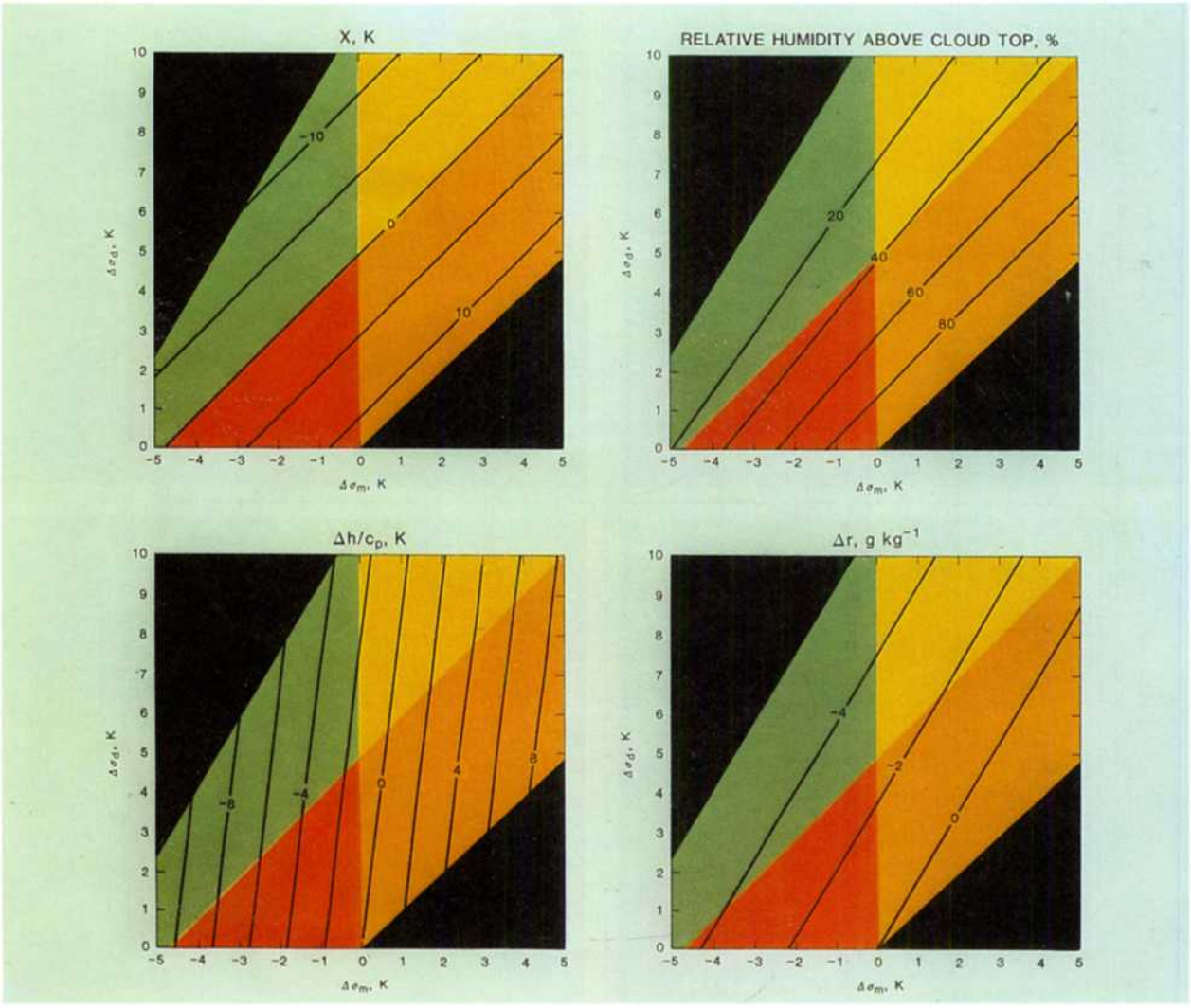

Fig. 3. As in Fig. 2, but for $\delta p_M = 150$ mb.

4. Second-order effects

How does entrainment tend to modify X itself? Considering only the time rates of change due to entrainment, we can show that

$$\frac{\partial X}{\partial t} = \frac{gE}{\delta p_M}(Y + \Gamma), \tag{4.1}$$

where

$$Y \equiv 2\Lambda_0 - X + D\left(\frac{\partial l_B}{\partial h_M}\right)\Delta h + D\left(\frac{\partial l_B}{\partial r_M}\right)\Delta r + D\left(\frac{\partial l_B}{\partial \delta p_M}\right)\delta p_M, \tag{4.2}$$

$$\Gamma \equiv -\delta p_M \left(\frac{L}{c_p}\right)\left[\frac{\partial l_B}{\partial h_M}\left(\frac{\partial h}{\partial p}\right)_{B+} + \frac{\partial l_B}{\partial r_M}\left(\frac{\partial r}{\partial p}\right)_{B+}\right], \tag{4.3}$$

$$D(\ ) = \frac{L}{c_p}\left[\Delta h \frac{\partial}{\partial h_M}(\ )\Delta r \frac{\partial}{\partial r_M}(\ ) + \delta p_M \frac{\partial}{\partial \delta p_M}(\ )\right]. \tag{4.4}$$

Both Y and Γ have the dimensions of temperature. To obtain (4.1), we have used (2.4) and

$$\frac{\partial \Delta h}{\partial t} = -gE\left[\left(\frac{\partial h}{\partial p}\right)_{B+} + \frac{\Delta h}{\delta p_M}\right], \tag{4.5}$$

$$\frac{\partial \Delta r}{\partial t} = -gE\left[\left(\frac{\partial r}{\partial p}\right)_{B+} + \frac{\Delta r}{\delta p_M}\right]. \tag{4.6}$$

Inspection of (4.3) shows that the Γ term of (4.1) represents the effects of the free atmospheric stratification on the time-rate-of-change of X. As discussed in Section 5, this term is generally negative. However, Y is typically positive, in part because $2\Lambda_0 - X$ is positive (see Section 2). Results presented in Section 5 suggest that $Y + \Gamma$ is often positive, so that entrainment tends to increase X.

5. Some examples

5.1. *Typical soundings*

According to McClatchey et al. (1972), the potential temperature and relative humidity soundings shown in Fig. 4 are "typical" for the tropical, mid-latitude summer, and subartic winter regions, respectively. The surface pressure is 1013 mb in each case. For each sounding, we can ask what will happen to a cloud as entrainment incorporates free atmospheric air into the mixed layer, while all other processes are inactive. To answer this question, it is not necessary to specify the rate of entrainment or

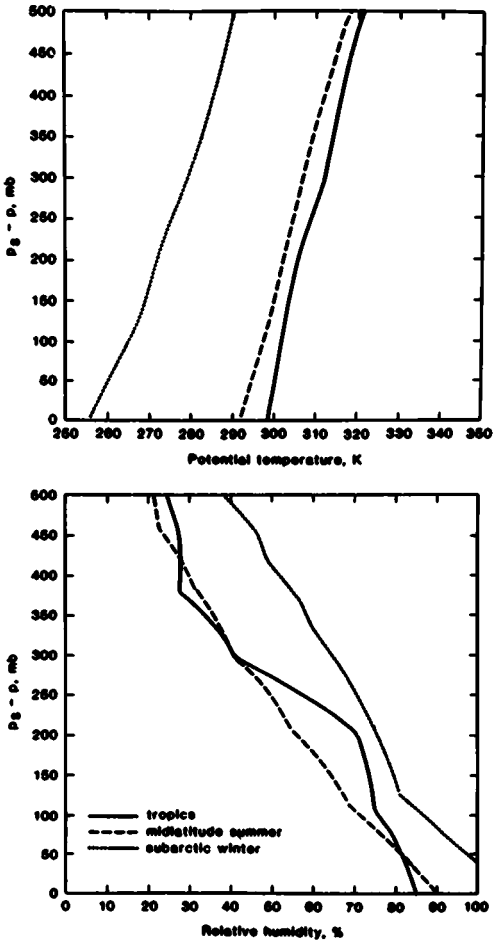

Fig. 4. Typical potential temperature and relative humidity profiles for the tropics, mid-latitude summer, and subarctic winter regions, according to McClatchey et al. (1972).

how this rate is determined. However, we must somehow assign values of δp_M, h_M, and r_M.

One possibility is to choose a value of δp_M, and define h_M and r_M by mass-weighted averaging of h and r over this portion of the sounding. Following this approach, we have considered increasing values of δp_M, in 1 mb increments, from 1 mb to 200 mb. For each value of δp_M, we have obtained the cloud depth, as well as X, $\Delta\sigma_d$, and $\Delta\sigma_m$. The results are shown in Fig. 5. The tropical and mid-latitude summer soundings yield cloud-free mixed layers until the mixed-layer depth reaches about 80mb, while the subartic winter sounding is cloudy from the beginning. CDE occurs for all three soundings, and X increases with δp_M, although Γ (not shown) is negative (see Section 4). The tropical and mid-latitude summer soundings have $\Delta\sigma_m < 0$, while the more stable subarctic winter sounding has $\Delta\sigma_m > 0$. All three soundings give $\Delta\sigma_d > 0$.

A second approach is to consider a range of δp_M, while holding h_M and r_M fixed at the respective surface values of h and r. This yields the results shown in Fig. 6. For these choices of δp_M,

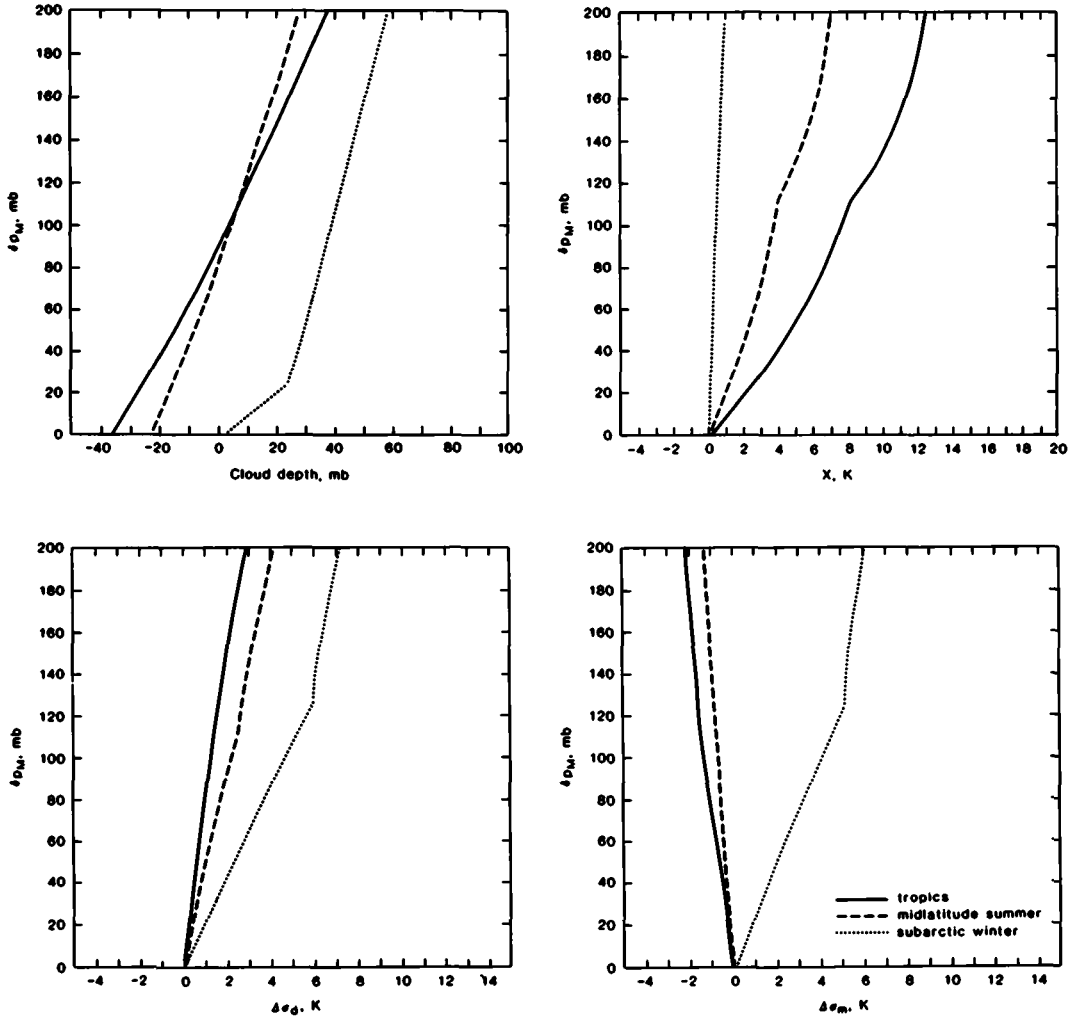

Fig. 5. Cloud depth, X, $\Delta\sigma_d$, and $\Delta\sigma_m$ as functions of δp_M, for the McClatchey soundings, where h_M and r_M are obtained by averaging the lower portions of the soundings through depth δp_M.

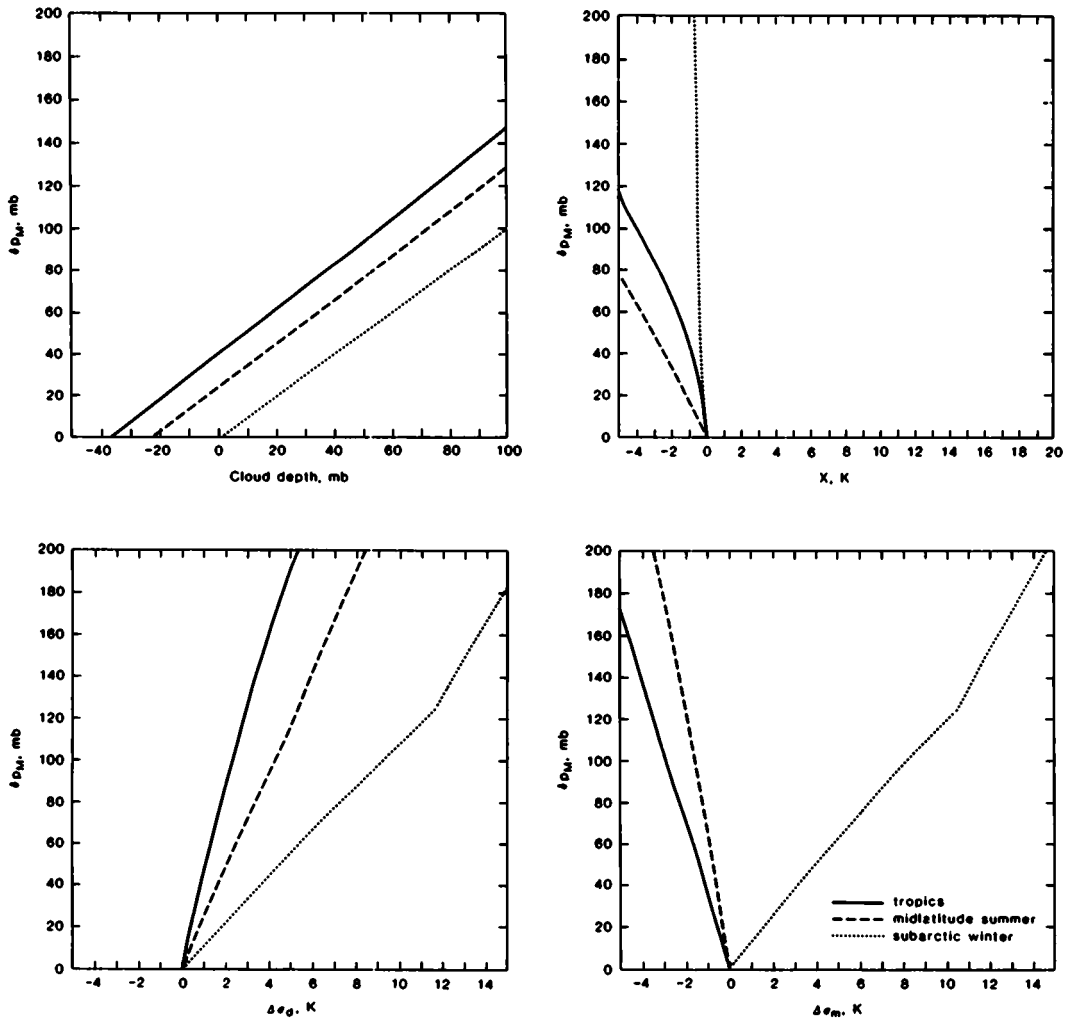

Fig. 6. Same as Fig. 5, except that h_M and r_M are set equal to the respective surface values of h and r, for each sounding.

h_M, and r_M, CDE does not occur with any of the three soundings.

5.2. *Neiburger's data*

Neiburger et al. (1961) (see also Neiburger (1960)) described ship observations of the structure of the marine layer over the eastern north Pacific Ocean in summer, including inversion-base and inversion-top values of the height, potential temperature, temperature, and relative humidity. We have used these data to plot the regional distributions of δp_M, X, $\Delta\sigma_m$ and inversion-base relative humidity shown in Fig. 7. CDE ($X > 0$) and cloud-top entrainment instability ($\Delta\sigma_m < 0$) both tend to occur in the south-west portion of the domain, where δp_M is relatively large. Near the coast, CDE and cloud-top entrainment instability do not occur.

5.3. *GCM results*

The UCLA general circulation model includes a parameterization of the planetary boundary layer in which the PBL depth is a prognostic variable. The time-evolution of the PBL is determined, in part, through an entrainment parameterization based on "Eulerian partitioning" (Randall, 1984). The PBL is assumed to be well-mixed, and the

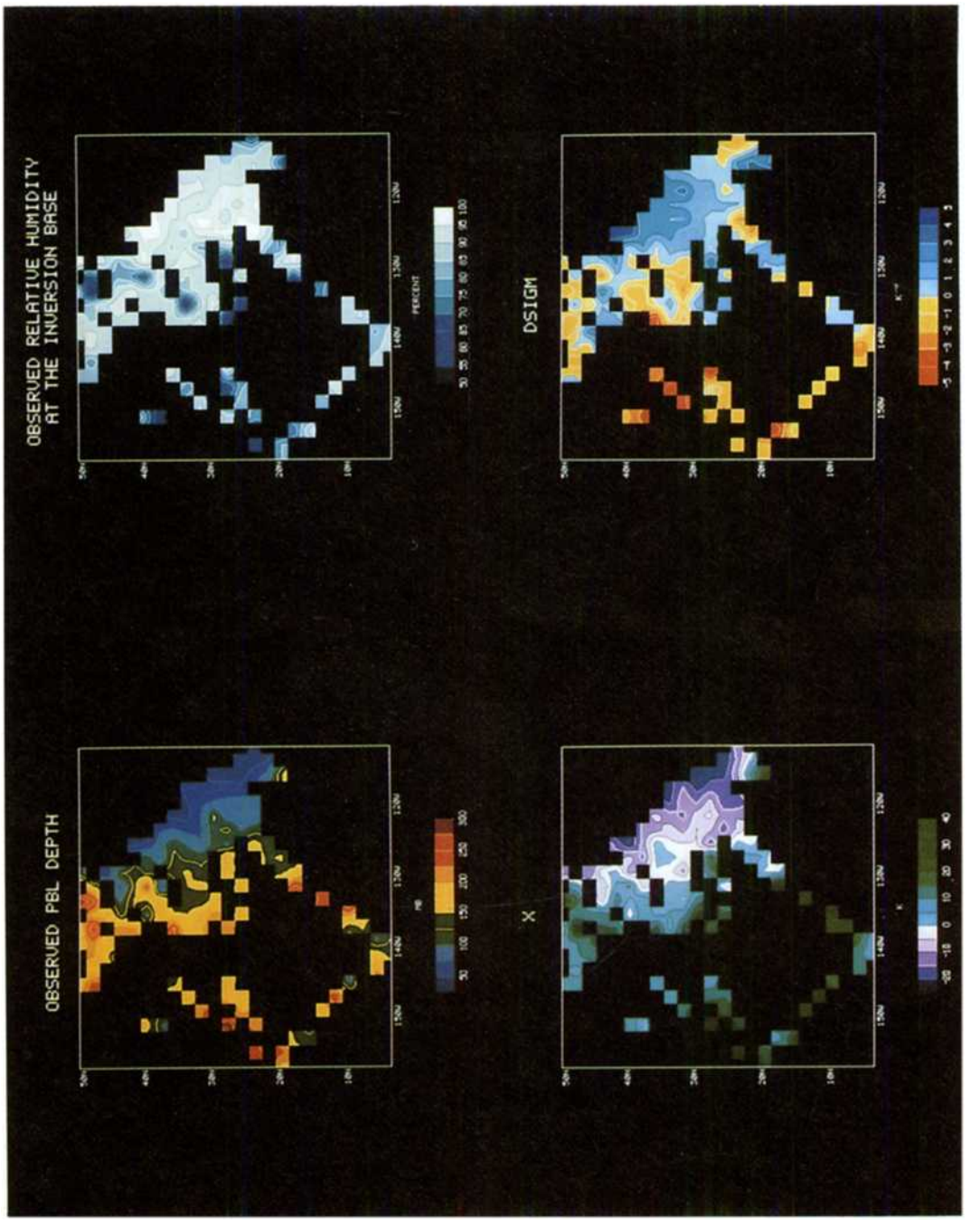

Fig. 7. Observed distributions of δp_M, X, $\Delta\sigma_M$ and the relative humidity at the inversion base, over the eastern north Pacific Ocean in summer, as derived from the data of Neiburger et al. (1961). In the lower right-hand panel, "DSIGM" refers to $\Delta\sigma_m$.

effects of PBL stratoculumus clouds are considered in the parameterizations of entrainment and radiation. The GCM also includes a crude parameterization of cloud-top entrainment instability; this is discussed further in the second paragraph below. A description of the GCM and some results are given by Suarez et al. (1983) and references therein.

We have investigated the rôle of CDE in the GCM by examining the global distribution of X in a particular time-step, chosen at random from a July history tape, in the middle of a multi-year simulation. In this time-step, CDE occurs over 18.8% of the earth's surface. Using the color scheme of Figs. 2 and 3, 10.5% of the earth is "red", 8.3% is "orange", 33.1% is "yellow", and 48.1% is "green". PBL stratus clouds cover 13.5% of the earth. At about a third of the stratus points (4.4% of the earth), the clouds are subject to cloud-top entrainment instability. About a fourth of these unstable stratus points (1.1% of the earth) are subject to CDE. Over a third of all stratus points (5.1% of the earth) are subject to CDE.

The widespread occurrence of CDE significantly influences the model's simulation of PBL stratocumulus clouds. The statistics given above show that CDE actually occurs much more frequently at stratus points than for the earth as a whole. The reason is that stratus-topped PBLs tend to be deep, and a deep PBL is favorable for CDE. The area-weighted average simulated PBL depth over all stratus points is 114 mb, while the average over all CDE stratus points is 166 mb. Although the GCM predicts that CDE sometimes occurs in conjunction with cloud-top entrainment instability, this result must be interpreted cautiously. In the design of the GCM, Suarez et al. (1983) assumed for simplicity that the onset of cloud-top entrainment stability leads to a rapid mixing of the PBL with the free atmosphere, and that during this process, the PBL depth does not change. The concept of a well-defined, entraining PBL was thus abandoned, without any real justification. As a result, the GCM as presently formulated cannot simulate the combined effects of CDE and the entrainment instability.

6. Summary and conclusions

An important consequence of CDE is that it can prevent the cloud-top entrainment instability from destroying a cloud deck. Without suppressing the instability, CDE transforms it from a cloud-destroyer to a cloud-builder. The examples discussed in Section 5 show that CDE is likely to be very common in nature, and that it must be properly taken into account in the design of cloud parameterizations for GCMs.

The analysis presented in this paper does not depend on an entrainment hypothesis. Moreover, it is not restricted to PBL stratocumulus sheets. Stratiform clouds in the free atmosphere can be subject to CDE; we need only reinterpret p_s as the pressure at the base of an elevated turbulent mixed layer. Modest departures from well-mixedness will alter the results quantitatively but not qualitatively. Processes other than entrainment, such as surface evaporation, radiative cooling, and advection will often work with CDE to build a cloud layer; but of course, advection in particular can also oppose CDE by reducing the relative humidity.

The weak assumption that the deepening of a cloud layer favors an increase in the cloud-top entrainment rate (without specifying any particular functional relationship) suggests the possibility of a positive feedback loop: a deeper cloud favors stronger entrainment, which feeds back positively (through CDE) to favor a deeper cloud. This would imply that CDE can cause rapid cloud growth, even in the absence of cloud-top entrainment instability.

Cloud-top entrainment is the *only* entrainment into a stratocumulus sheet, and in this paper the analysis has focused on the cloud-topped mixed layer. However, some of the concepts presented in this paper may be applicable to cumulus cloud-top entrainment.

7. Acknowledgements

A portion of this research was performed while David Randall was visiting the International Meteorological Institute at the University of Stockholm. The hospitality of Dr. Hilding Sundqvist and Professor Bert Bolin is gratefully acknowledged.

Thanks are due to Professor Akio Arakawa of UCLA for helpful comments. Mary Ann Wells typed the manuscript, and Laura Rumberg drafted the figures. Jim Abeles, Ernie Pittarelli and Tom Corsetti assisted with the computer programming.

8. Appendix

Cloud-top liquid water mixing ratio

The method presented here is based on that used by Suarez et al. (1983).

Let $q^*(T, p)$ be the saturation value of the water vapor mixing ratio, q, In the following, $\mathrm{d}/\mathrm{d}p$ denotes a derivative with respect to pressure, at constant horizontal coordinates and time. In general,

$$\frac{\mathrm{d}q^*}{\mathrm{d}p} = \left(\frac{\partial q^*}{\partial T}\right)_p \frac{\mathrm{d}T}{\mathrm{d}p} + \left(\frac{\partial q^*}{\partial p}\right)_T. \tag{A.1}$$

When θ is constant in height, as shown by the dotted line in Fig. 8, eq. (A.1) becomes

$$\frac{\mathrm{d}q^*}{\mathrm{d}p} = \frac{\gamma}{\rho L} + \left(\frac{\partial q^*}{\partial p}\right)_T, \tag{A.2}$$

where ρ is the density, and $\gamma \equiv (L/c_p)(\partial q^*/\partial T)_p$.

Using T_{BO} (see Fig. 8), given by

$$T_{BO} = \left(\frac{p_B}{p_S}\right)^{\kappa} (h_M - L r_M)/c_p, \tag{A.3}$$

we define

$$q^*_{BO} \equiv q^*(T_{BO}, p_B). \tag{A.4}$$

The liquid water mixing ratio at cloud top is approximately given by

$$l_B = r_M - q^*_{BO}. \tag{A.5}$$

We find from (A.3) and (A.5) that

$$L\left(\frac{\partial l_B}{\partial h_M}\right)_{r_M, \delta p_M} = -\gamma_B \left(\frac{p_B}{p_S}\right)^{\kappa}, \tag{A.6}$$

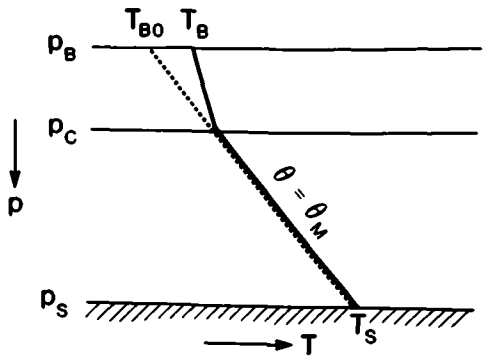

Fig. 8. Diagram illustrating the method used to determine cloud depth and cloud-top liquid water mixing ratio. The pressures at the cloud top, cloud base, and earth's surface are denoted by p_B, p_C, and p_S, respectively. The solid line shows the temperature profile, which is dry adiabatic in the subcloud layer and moist adiabatic in the cloud layer. The surface temperature T_S and the cloud-top temperature T_B lie along this solid line. The dashed line shows a continuation of the dry adiabatic lapse rate into the cloud layer. We define T_{BO} as the temperature along this dashed line, where it reaches cloud top.

$$\left(\frac{\partial l_B}{\partial r_M}\right)_{h_M, \delta p_M} = 1 + \gamma_B \left(\frac{p_B}{p_S}\right)^{\kappa}, \tag{A.7}$$

and (compare with (A.2))

$$\left(\frac{\partial l_B}{\partial \delta p_M}\right)_{h_M, r_M} = \frac{\gamma_B}{\rho_B L} + \left[\left(\frac{\partial q^*}{\partial p}\right)_T\right]_B. \tag{A.8}$$

In (A.8), the γ_B term dominates.

REFERENCES

Brost, R. A., Lenschow, D. H. and Wyngaard, 1982. Marine stratocumulus layers. Part I: Mean conditions, *J. Atmos. Sci. 39*, 800–817.

Chen, Chiang and Cotton, W. R. 1983. A one-dimensional simulation of the stratocumulus-capped mixed layer. *Boundary Layer Meteorol. 25*, 289–322.

Deardorff, J. W. 1980. Cloud-top entrainment instability. *J. Atmos. Sci. 37*, 131–147.

Lilly, D. K. 1968. Models of cloud-topped mixed layers under a strong inversion. *Q. J. R. Meteorol. Soc. 94*, 292–309.

Mahrt, L. and Paumier, J. 1982. Cloud-top entrainment instability observed in AMTEX. *J. Atmos. Sci. 38*, 622–634.

McClatchey, R. A., Fenn, R. W., Selby, J. E. A., Volz, F. E. and Garing, J. S. 1972. *Optical properties of the atmosphere* (3rd edition). AFCRL-047297, 108 pp (NTIS # AD753075).

Moeng, C.-H. and Arakawa, A. 1980. A numerical study of a marine subtropical stratus cloud layer and its stability. *J. Atmos. Sci. 37*, 2661–2676.

Neiburger, M. 1960. The relation of air mass structure to

the field of motion over the eastern north Pacific Ocean in summer. *Tellus 12*, 31–40.

Neiburger, M., Johnson, D. S. and Chien, C.-W. 1961. *Studies of the structure of the atmosphere over the eastern Pacific Ocean in summer (I). The inversion over the eastern north Pacific Ocean.* University of California Press, Berkeley and Los Angeles.

Randall, D. A. 1980. Conditional instability of the first kind, upside-down. *J. Atmos. Sci. 37*, 125–130.

Randall, D. A. 1984. Buoyant production and consumption of turbulence kinetic energy in cloud-topped mixed layers. *J. Atmos. Sci. 41*, 402–413.

Suarez, M. J., Arakawa, A. and Randall, D. A. 1983. The parameterization of the planetary boundary layer in the UCLA general circulation model: formulation and results. *Mon. Weather Rev. 111*, 2224–2243.